General Disclaimer

One or more of the Following Statements may affect this Document

- This document has been reproduced from the best copy furnished by the organizational source. It is being released in the interest of making available as much information as possible.

- This document may contain data, which exceeds the sheet parameters. It was furnished in this condition by the organizational source and is the best copy available.

- This document may contain tone-on-tone or color graphs, charts and/or pictures, which have been reproduced in black and white.

- This document is paginated as submitted by the original source.

- Portions of this document are not fully legible due to the historical nature of some of the material. However, it is the best reproduction available from the original submission.

NASA Technical Memorandum 83451

Semidirect Computations for Transonic Flow

(NASA-TM-83451) SEMIDIRECT COMPUTATIONS FOR TRANSONIC FLOW (NASA) 15 p HC A02/MF A01 CSCL 01A
N83-34909
Unclas
G3/02 42050

Julie M. Swisshelm and John J. Adamczyk
Lewis Research Center
Cleveland, Ohio

Prepared for the
Sixth Computational Fluid Dynamics Conference
sponsored by the American Institute of Aeronautics and Astronautics
Danvers, Massachusetts, July 13-15, 1983

NASA

SEMIDIRECT COMPUTATIONS FOR TRANSONIC FLOW

Julie M. Swisshelm and John J. Adamczyk

National Aeronautics and Space Administration
Lewis Research Center
Cleveland, Ohio 44135

E-1765

ABSTRACT

A semidirect method, driven by a Poisson solver, has been developed for inviscid transonic flow computations. It is an extension of a recently introduced algorithm for solving subsonic rotational flows. Shocks are captured by implementing a form of artificial compressibility. Nonisentropic cases are computed using a shock tracking procedure coupled with the Rankine-Hugoniot relationships. Results are presented for both subsonic and transonic flows. For the test geometry, an unstaggered cascade of 20 percent thick circular arc airfoils at zero angle of attack, shocks are crisply resolved in supercritical situations and the algorithm converges rapidly. In addition, the convergence rate appears to be nearly independent of the entropy and vorticity production at the shock.

INTRODUCTION

Semidirect algorithms are constructed by incorporating a direct solver into an iterative procedure. For transonic flows, one of the first publications on this topic is Lomax and Martin(1). There, the governing equation was the small disturbance transonic flow equation. Jameson(2) developed a semidirect solver for the potential flow equation. It was based on a direct solver for a Poisson equation. For subcritical flows this algorithm exhibited good convergence; however, when the flow became supercritical convergence of the scheme could not be achieved without the injection of line relaxation.

More recently, a general methodology for constructing such schemes for the equations of fluid motion was advanced by Martin(3). The applications in his paper, however, were restricted to incompressible and subsonic two-dimensional potential flows. Chang and Adamczyk(4) have succeeded in extending the scheme suggested by Martin for solving two-dimensional potential flows to three-dimensional inviscid subsonic rotational flows.

In the present paper, Chang and Adamczyk's method is extended to the computation of supercritical flows. The satisfaction of both the continuity equation and the vorticity-velocity kinematic relation is achieved by recursively applying a direct solver to two Poisson equations in computational space. For isentropic flows, shocks are captured by implementing the artificial compressibility technique presented by Hafez, South, and Murman(5). The algorithm is also capable of treating flows with nonisentropic shocks by adding a shock-tracking operator coupled with the Rankine-Hugoniot relations.

Numerical experiments conducted during the development of the present algorithm showed that the asymptotic convergence history was governed by a real eigenvalue. This implied that the algorithm could be accelerated by a power method as suggested by the work of Hafez and Cheng[6].

Convergence histories are presented for the unaccelerated and accelerated form of the algorithm. These results include inviscid subcritical and supercritical potential and nonpotential flows. In addition the Mach number distributions associated with a cascade of unstaggered 20 percent thick circular arc airfoils operating at subcritical and supercritical conditions are presented.

ALGORITHM FORMULATION

Steady Potential Flow

In steady potential flow calculations, flows are assumed to be isentropic and isoenergetic, implying irrotationality. This assumption has proven useful in approximating many real flow situations.

The differential equations governing potential flow are:

$$\vec{\nabla} \cdot (\rho\vec{U}) = 0 \tag{1}$$

$$\vec{\nabla} \times \vec{U} = 0 \tag{2}$$

where ρ is the density and $\vec{U}$ is the velocity vector. Equation (1) represents the continuity equation and equation (2) the irrotationality condition. A thermodynamic relationship which expresses density in terms of velocity is:

$$\rho = \frac{P_o}{RT_o}\left[1 - \frac{U^2}{2\,C_pT_o}\right]^{\frac{1}{\gamma-1}} \tag{3}$$

where P_o, T_o, R, C_p, γ and U^2 are total pressure, total temperature, the ideal gas constant, the specific heat capacity at constant pressure, the ratio of specific heat capacities, and the speed squared, respectively.

The solution procedure for subcritical flows is defined by the following set of equations[4], written in tensor form:

$$\frac{\partial^2\varphi^{(n)}}{\partial x^k\,\partial x^k} = -\frac{\partial F^{k(n-1)}}{\partial x^k} \tag{4}$$

$$\bar{F}^k = F^{k(n-1)} + \frac{\partial\varphi^{(n)}}{\partial x^k} \tag{5}$$

$$\tilde{U}_k = g_{kl}\bar{F}^{l(n)}/\sqrt{g}\,\rho^{(n-1)} \tag{6}$$

$$\frac{\partial^2\sigma^{(n)}}{\partial x^k\,\partial x^k} = \frac{\partial}{\partial x^k}\left(\tilde{U}_k - U_k^{(n-1)}\right) \tag{7}$$

$$U_k^{(n)} = U_k^{(n-1)} + \frac{\partial\sigma^{(n)}}{\partial x^k} \tag{8}$$

$$\rho^{(n)} = \frac{P_o}{RT_o}\left[1 - \frac{g^{kl}U_k^{(n)}U_l^{(n)}}{2\,C_pT_o}\right]^{\frac{1}{\gamma-1}} \tag{9}$$

$$F^{k(n)} = \sqrt{g}\;g^{kl}\rho^{(n)}U_k^{(n)} \tag{10}$$

where F^k, U_k, g^{kl}, g_{kl}, g and x^k are the contravariant mass flux vector density, the covariant velocity component, the contravariant metric tensor, the covariant metric tensor, the determinant of the covariant metric tensor, and the computational coordinates, respectively. The use of repeated indices denotes the standard summation convention of tensor analysis. For three-dimensional flows the free index k takes on the value of 1, 2, and 3, while for two-dimensional flows its values are restricted to 1 and 2. The variables φ and σ are interpreted as scalar correction quantities. Equations (4), (5), and (6) satisfy the continuity equation (1), generating the vector F^k which is divergence free. Likewise, equations (7) and (8) generate a vector U_k which satisfies the irrotationality condition (eq. 2). This algorithm can be thought of as a two-step recursive scheme in which the first step generates a solution to the continuity equation while leaving the irrotationality condition unsatisfied. The second step corrects the intermediate velocity field so as to satisfy the irrotationality condition. Upon convergence, the intermediate vector $\tilde{U}_k$ approaches $U_k^{(n)}$. The implementation of the above algorithm requires the solution of two Poisson equations (i.e., eqs. (4) and (7)) in computational space for each iteration cycle. These equations are readily solved by direct solvers or fast Poisson solvers.

The iteration procedure is initialized by assuming a uniform covariant velocity field and constant density, which is sufficient to determine the quantity $F^{k(n-1)}$. Applying a direct solver to equation (4), the scalar φ is computed for the entire flowfield. Intermediate values of the mass flux vector, $\bar{F}^k$, and the velocity vector, $\tilde{U}_k$, are calculated by equations (5) and (6). The direct solver is then invoked a second time to find the σ field which satisfies equation (7). The corrected velocity vector $U_k^{(n)}$ is then determined from equation (8). At this point the density is updated using equation (9) and the current velocity. The mass flux vector $F^{k(n)}$ is recomputed according to equation (10) and returned to equation (4), which initiates the next cycle of the iteration scheme.

Global conservation of mass is maintained by staggering the variables on the computational mesh. As shown in figure 1, the quantities φ and σ are placed at the $(i,j)^{th}$ mesh points, while all other variables (such as ρ, U_k, and s) are calculated at the center of each mesh cell side. For equations (5) and (8), in which F^k and U_k are computed using the correction variables φ and σ, the differencing scheme is :

$$A^1_{i+\frac{1}{2},j} = \frac{B_{i+1,j} - B_{i,j}}{\Delta x^1} \tag{11}$$

$$A^1_{i,j+\frac{1}{2}} = \frac{\frac{1}{2}\left(B_{i+1,j} + B_{i+1,j+1}\right) - \frac{1}{2}\left(B_{i-1,j} + B_{i-1,j+1}\right)}{\Delta x^1} \tag{12}$$

$$A^2_{i+\frac{1}{2},j} = \frac{\frac{1}{2}\left(B_{i,j+1} + B_{i+1,j+1}\right) - \frac{1}{2}\left(B_{i,j-1} + B_{i+1,j-1}\right)}{\Delta x^2} \tag{13}$$

$$A^2_{i,j+\frac{1}{2}} = \frac{B_{i,j+1} + B_{i,j}}{\Delta x^2} \tag{14}$$

where A^k and B represent F^k and φ for equation (5) and, similarly, U_k and σ for equation (8).

In transonic flow computations, artificial compressibility is employed as a shock-capturing procedure. Density is modified by an upwinded differencing procedure, according to the equation:

$$\tilde{\rho}_{i,j} = \bar{\rho}_{i,j} + \alpha\mu_{i,j}\left(\bar{\rho}_{i-1,j} - \bar{\rho}_{i,j}\right) \tag{15}$$

where

$$\mu_{i,j} = \max\left[1 - \left(\frac{1}{M^2_{i,j}}\right), 0\right]$$

and where α is a constant of order 1. The variable $M_{i,j}$ is the Mach number at the $(i,j)^{th}$ mesh point. The quantity $\tilde{\rho}_{i,j}$ replaces the density in the calculation of the flux and the velocity vector. It should be noted that in adapting this form of artificial compressibility we have assumed that the streamwise grid lines (x^2 = constant) nearly coincide with the streamlines. A similar procedure is applied to the speed squared, q^2, to damp a Mach number overshoot that occurs immediately upstream of the shock:

$$\bar{q}^2_{i,j} = q^2_{i,j} + \alpha' \mu_{i,j} \left(q^2_{i-1,j} - q^2_{i,j} \right) \tag{16}$$

where

$$q^2 = g^{kl} U_k U_l$$

The coefficients μ and α' are the same as defined previously, q^2 is the speed squared, and $\bar{q}^2$ replaces q^2 in equation (9) for the density calculation.

The measures of convergence, or the "residuals" of the computation, are taken to be the magnitudes of the quantities $\nabla \cdot (\rho\vec{U})$ and $\nabla \cdot (\tilde{U} - \vec{U}^{(n-1)})$. Both of these are driven to zero by the iteration procedure. Upon convergence the vector F^k will be divergence free and U_k irrotational as prescribed by the governing equations.

Nonisentropic Flow

The potential flow formulation is extended to permit the computation of two-dimensional isoenergetic flows with nonisentropic shocks. This is accomplished by introducing a shock-tracking operator coupled with the Rankine-Hugoniot relationships and the entropy transport equation.

The governing equations for inviscid, isoenergetic flows with nonisentropic shocks are:

$$\vec{\nabla} \cdot (\rho\vec{U}) = 0 \tag{17}$$

$$\omega = \vec{\nabla} \times \vec{U} \tag{18}$$

$$\vec{U} \cdot \vec{\nabla}S = 0 \tag{19}$$

and the thermodynamic relationship

$$\rho = \frac{P_o}{RT_o} \left[1 - \frac{U^2}{2\, C_p T_o} \right]^{\frac{1}{\gamma-1}} \tag{20}$$

The nonisentropic iteration scheme is basically the same as that for isentropic flow, with some modifications to be mentioned below. Density, as defined by equation (15), is reevaluated for the nonisentropic case according to the expression:

$$\hat{\rho} = \bar{\rho}\, e^{-(S-S_o)/C_v} \tag{21}$$

where C_V is the specific heat capacity at constant volume, and $(S-S_O)$, the entropy rise across the shock, is obtained from the Rankine-Hugoniot relationship:

$$S - S_o = \frac{\gamma R}{\gamma - 1} \ln \frac{p_2}{p_1}\frac{\rho_1}{\rho_2} - R \ln \frac{p_2}{p_1} \tag{22}$$

which, when written solely in terms of M_n, the Mach number normal to the shock, becomes

$$\frac{S - S_o}{R} = \ln \left\{ \left[1 + \frac{2\gamma}{\gamma + 1}\left(M_n^2 - 1\right)\right]^{1/(\gamma-1)} \left[\frac{(\gamma + 1)M_n^2}{(\gamma - 1)M_n^2 + 2}\right]^{\gamma/(\gamma-1)} \right\} \tag{23}$$

The switching operator $\mu_{i,j}$ defined earlier is used to track the shock location and its geometry. If we consider the flow to have a uniform entropy distribution across the inlet, the shock provides the only mechanism by which entropy can be introduced into the field. So introduced, the entropy (according to eq. (19)) will remain constant along streamlines downstream of the shock. Since we have assumed the grid line x^2 = constant nearly approximates a streamline, the entropy will be held constant along each streamwise grid line downstream of the shock. Once the entropy field is established, the density is reevaluated according to equation (21). The vorticity field generated by the shock may be computed from the following equation[7]:

$$\frac{\omega}{p} = \frac{d\left(\frac{S}{R}\right)}{d\psi} \tag{24}$$

where ω, p, and x^2 are the vorticity, the pressure (which is related to density and entropy by the ideal gas equation of state), and the transverse computational coordinate, respectively. The vorticity field is used to construct a covariant vector whose only component is $A_1^{(n)}$ (i.e., $A_2^{(n)} = 0$) according to

$$A_1^{(n)} = \int \omega \sqrt{g}\, dx^2 \tag{25}$$

One should note that the curl of the constructed covariant vector is equal to ω. By adding the quantity $\left(A_1^{(n)} - A_1^{(n-1)}\right)$ to $U_1^{(n)}$ at the end of each iteration cycle the resulting velocity field upon convergence will satisfy equation (18).

For subsonic flows the stability bounds of the current algorithm were defined by Chang and Adamczyk[4]. Based on this analysis and a series of computational experiments it appeared that the asymptotic convergence rate of the current algorithm is determined by a real eigenvalue. This implies that the algorithm can be accelerated by a simple application of the power method as outlined by Hafez and Cheng[6]. To analyze this acceleration procedure let λ denote the dominant eigenvalue, and assume that the asymptotic convergence history of the current algorithm is governed by the equation:

$$\varepsilon^{k+1} = \lambda \varepsilon^{k} \tag{26}$$

where ε^k is the error vector at the end of the k^{th} iteration cycle. For the present analysis ε^k is defined as:

$$\varepsilon^{k} = B^{k} - B \tag{27}$$

where B^k represents the value of the unknown vector B at the end of the k^{th} iteration cycle. The value of λ may be estimated from the equation:

$$\lambda = \Sigma\left|B^{k+1} - B^{k}\right| / \Sigma\left|B^{k} - B^{k-1}\right| \tag{28}$$

where Σ denotes the summation over all components of B. With λ known the limit of B^k is estimated by means of the equation:

$$B = B^{k} + \frac{B^{k+1} - B^{k}}{1 - \lambda} \tag{29}$$

Numerical results will show that this simple acceleration procedure is most effective in accelerating the current iteration procedure.

RESULTS

The algorithm has been tested for both subsonic and transonic flows through a two-dimensional straight channel with a 10 percent thick circular arc airfoil mounted on one wall. This simulates a cascade of 20 percent thick unstaggered circular arc airfoils at zero angle of attack. The computational grid, shown in figure 2, with 60 mesh intervals in the lengthwise direction and 16 intervals in the transverse direction, is orthogonal at the boundaries, as required by the present treatment of boundary conditions in the Poisson solver. The Poisson solver used in this study was constructed using block tridiagonal inversion. The boundary conditions required the specification of the mass flow at the inlet and the flow angle at the exit. Along the walls of the channel flow tangency was required.

Potential Flow Results

The results for the isentropic flow computations are shown in figures 3 and 4. For the subcritical case with an inlet Mach number of 0.5, the isomach distribution in the channel and the Mach number along the upper and lower walls are shown in figures 3(a) and (b), respectively. Both figures illustrate the symmetry of the computed flowfield about midchord of the airfoil.

The convergence measures, defined earlier as the divergences of the vectors $(\rho\vec{U})$ and $\tilde{U} - \vec{U}^{(n-1)}$ at each grid point, are shown in figure 3(c), which shows the average value of $\nabla \cdot (\rho\vec{U})$ at each iteration for the unaccelerated and accelerated versions of the algorithm. The convergence history of $\nabla \cdot \left(\tilde{U} - \vec{U}^{(n-1)}\right)$ exhibits similar behavior, meaning that the algorithm converges to the correct limit. The residual of the accelerated computation has been reduced ten orders of magnitude in about 50 iterations.

For the supercritical isentropic flow case, an inlet Mach number of 0.675 causes the formation of a shock in the channel at about 75 percent of the airfoil chord as illustrated by the isomach contour distribution of figure 4(a). The shock is resolved between two consecutive grid points, as one can see from the plot of surface Mach number in figure 4(b). The unaccelerated and accelerated convergence histories of the divergence of the mass flux vector are plotted in figure 4(c). The accelerated version is reduced ten orders of magnitude in 90 iterations.

Nonisentropic Flow Results

For the nonisentropic computations, a uniform entropy distribution across the inlet is assumed. Hence subcritical computational results are identical to those of the isentropic case displayed earlier. In supercritical flows the shock is tracked by monitoring the switching operator for large variations. By assuming the shock orientation to be normal to the streamwise gridlines, the resulting entropy rise across the shock is calculated. The flowfield resulting from an inlet Mach number of 0.675 is illustrated by the isomach contours in figure 5(a). The corresponding distribution of Mach number along the walls is plotted in figure 5(b). One can see from these figures that the inclusion of entropy and vorticity in the iterative scheme alters the shock strength slightly from that of potential flow, which in turn affects the flow downstream. The convergence histories of accelerated and unaccelerated computations, shown in figure 5(c), show that the residual is reduced ten orders of magnitude in 110 iterations. The nonisentropic flow convergence rate is slightly slower than that for potential flow.

CONCLUSIONS

A semidirect method for applications to transonic flows with shocks has been presented.

The ability of the algorithm to resolve flows modelled by the potential equation and the Euler equations for flows with constant total enthalpy is demonstrated for subcritical as well as shocked supercritical flows.

The applicability of the scheme to these cases has been sustantiated by the computational results presented in this paper. Shocks are resolved sharply and the resulting flowfields compare favorably to those obtained by others for the same problem.

For the standard, or unaccelerated, version of the algorithm, converged solutions were attained in 130 to 210 iterations. By accelerating the solver using a procedure which annihilates the dominant eigenvalue, the number of cycles is reduced to between 50 and 170 for the same convergence criteria.

REFERENCES

1. Lomax, Harvard, and Martin, E. Dale: "Fast Direct Numerical Solution of the Nonhomogeneous Cauchy-Riemann Equations," Journal of Computational Physics, Vol. 15, Aug. 1973, pp. 55-80.

2. Jameson, Antony: "Transonic Potential Flow Calculations Using Conservation Form," Proc. AIAA 3rd Computational Fluid Dynamics Conf., Hartford, CT, June 1975.

3. Martin, E. D.: "A Split-Recoupled-Semidirect Computational Technique Applied to Transonic Flow Over Lifting Airfoils," AIAA Paper 78-11, Jan. 1978.

4. Chang, Sin-Chung, and Adamczyk, John J.: "A Semi-Direct Solver for Compressible Three-Dimensional Rotational Flow," AIAA Paper 83-1909, July 1983.

5. Hafez, M., South, J., and Murman, E. M.: "Artificial Compressibility Methods for Numerical Solutions of Transonic Full Potential Equation," AIAA Journal, Vol. 17, Aug. 1978, pp. 838-844.

6. Hafez, M. M., and Cheng, H. K.: "Convergence Acceleration and Shock Fitting For Transonic Aerodynamics Computations," Univ. Southern Calif., Los Angeles, Calif., NR 061-192, Apr. 1975.

7. Von Mises, Richard: Mathematical Theory of Compressible Fluid Flow. Academic Press, Inc., New York, 1958, p. 426.

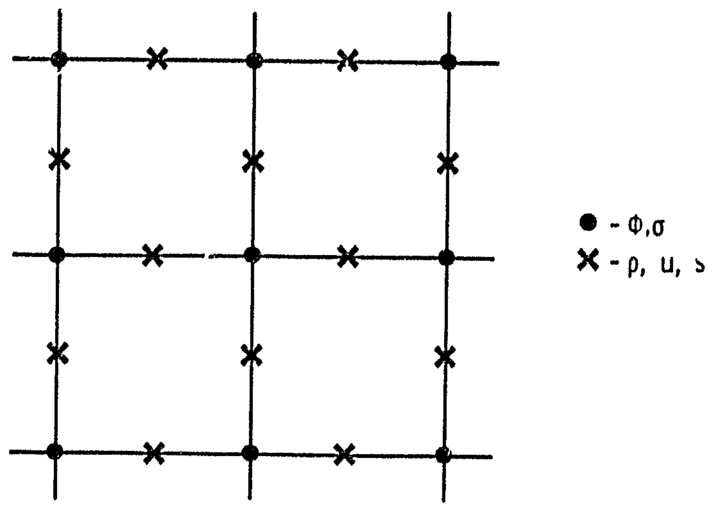

Figure 1. - Grid staggering.

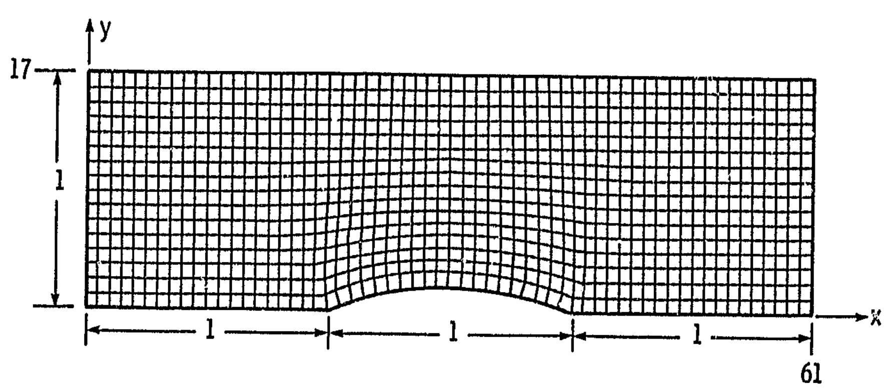

Figure 2. - Computational mesh.

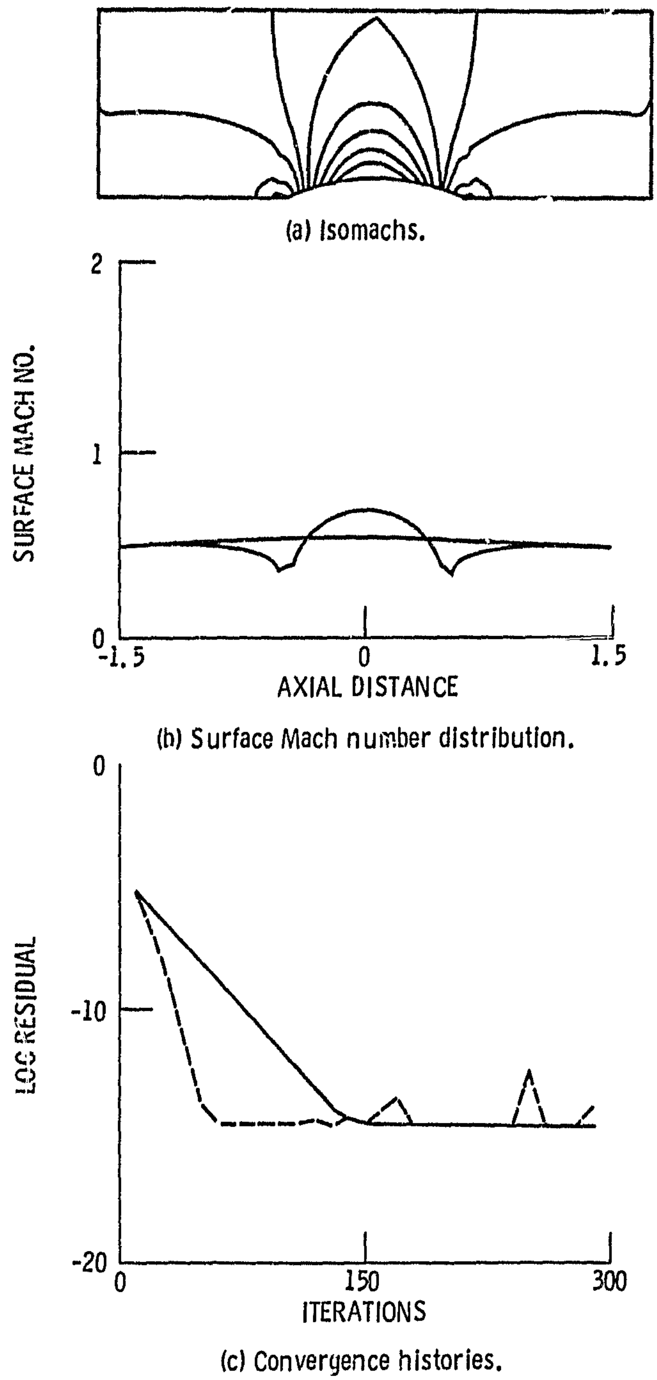

Figure 3. - Subcritical flow case, inlet Mach number = 0.5.

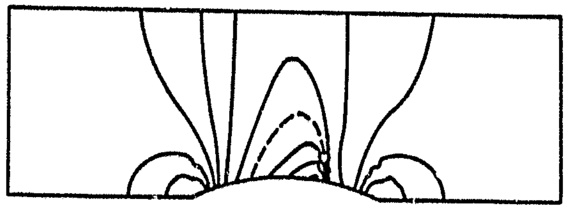

(a) Isomachs.

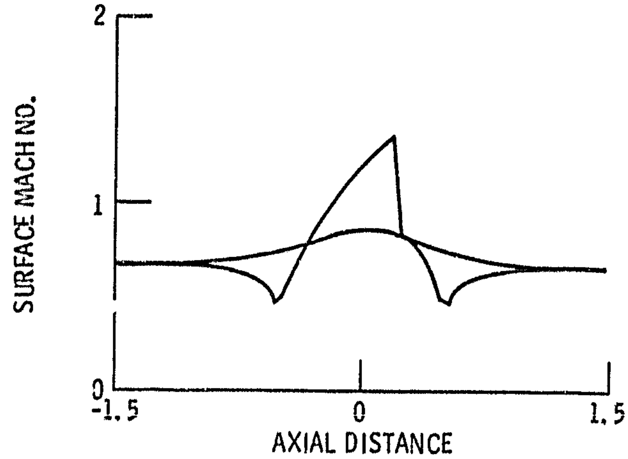

(b) Surface Mach number distribution.

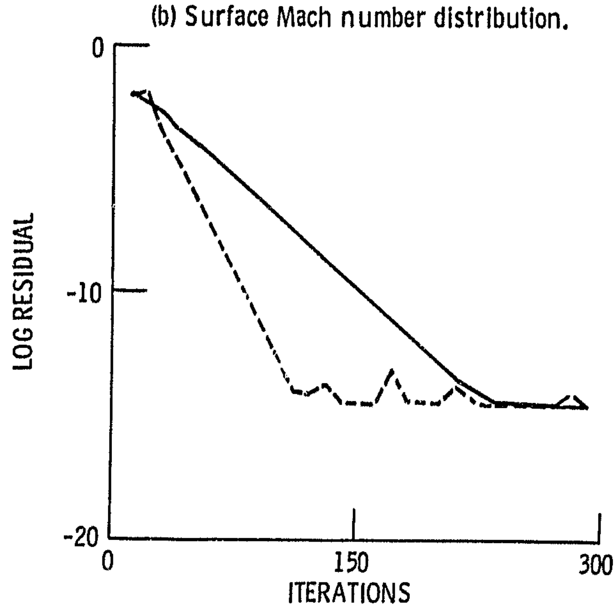

(c) Convergence histories.

Figure 4. - Supercritical isentropic, irrotational flow case, $M_\infty = 0.675$.

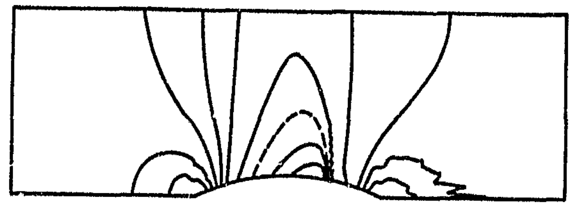

(a) Isomachs.

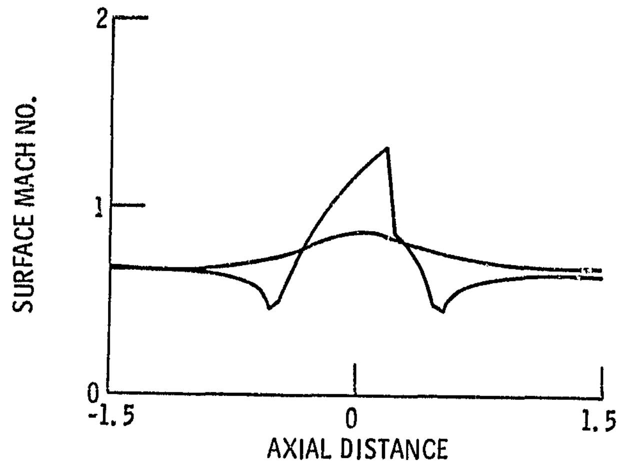

(b) Surface Mach number distribution.

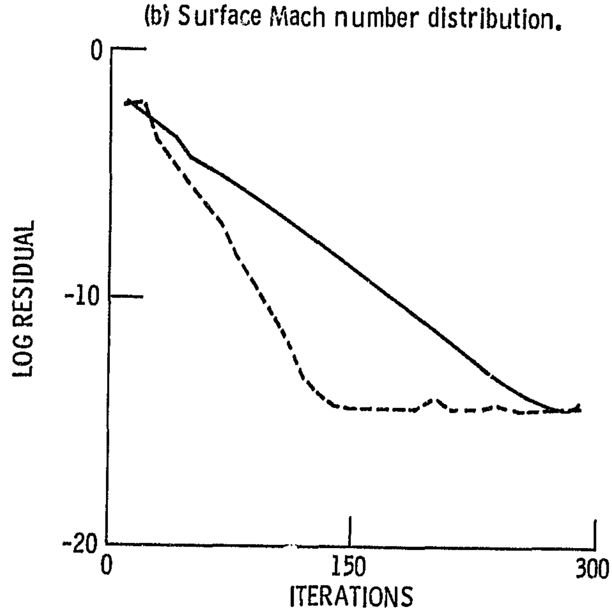

(c) Convergence histories.

Figure 5. - Supercritical nonisentropic rotational flow case, $M_\infty = 0.675$.